CURRENT EFFECTS ON NONLINEAR INTERACTIONS OF SHALLOW-WATER WAVES

By Qin Chen,[1] Associate Member, ASCE, Per A. Madsen,[2] and David R. Basco,[3] Member, ASCE

ABSTRACT: This study focuses on the effects of depth-uniform currents on near-resonant triad interactions of gravity waves in shallow water. First, we derive the evolution equations for triad interactions based on Yoon and Liu's equations with a constant water depth and an ambient current. An opposing current increases the magnitude of phase mismatch, resulting in a reduction of the degree of interactions and vice versa for a following current. Second, numerical experiments on harmonic generation and nonlinear shoaling of shallow-water waves with opposing and following currents are given by the use of an enhanced Boussinesq model with higher dispersion accuracy for wave/current interaction. The numerical model predictions that are in good agreement with the physical experiment data in the absence of ambient currents serve as a benchmark to reveal the current effects on nonlinear interactions of shallow-water waves. Although an opposing current increases wave heights, it actually reduces the Ursell number, beat-length, and ratio of the energy in higher harmonics to the energy in the primary wave in comparison with the pure wave motion in shallow water. Conversely, it is found that a following current intensifies the extent of triad interactions. This is in contrast to the current influence on quadruplet interactions of deepwater waves.

INTRODUCTION

When wind waves propagate into nearshore regions from deep ocean, quadruple resonance [see Phillips (1960) and Hasselmann (1962)] becomes much weaker in comparison with triad interactions in shallow water. Nonlinear interactions of shallow-water waves result in significant cross-spectral energy transfers over a distance of several hundred meters, as observed by Freilich and Guza (1984). Armstrong et al. (1962) and Bretherton (1964) introduced the concept of near resonance for weakly nonlinear systems, and showed that energy transfers among the wave components occur if the resonance conditions are only approximately satisfied, or

$$\pm\mathbf{k}_1 \pm \mathbf{k}_2 \mp \mathbf{k}_3 = \delta^+ \tag{1}$$

$$\pm\omega_1 \pm \omega_2 \mp \omega_3 = \delta^- \tag{2}$$

in which $\mathbf{k}_i$ and ω_i (i = 1, 2, 3) = wave-number vectors and the angular frequencies corresponding to three wave components, respectively. For dispersive gravity waves, $\delta^+ \neq 0$ while $\delta^- \equiv 0$. The near-resonance conditions for interactions of a wave component with its second harmonic may be expressed by

$$k_2 - 2k_1 = \delta_2 \tag{3}$$

$$\omega_2 - 2\omega_1 = 0 \tag{4}$$

where δ_2 = so-called mismatch between the wave numbers of the free and bound second harmonics.

The simplest example of near-resonant triad interactions of shallow-water waves is most likely the harmonic generation on a flat bottom when first-order boundary conditions are applied. The use of the first-order wave input in physical or nonlinear numerical models leads to the release of parasitic higher harmonics that are of equal amplitude and opposite phase compared with the bound higher harmonics. The mismatch between bound and free wave numbers governs the so-called beat-length, where energy may exchange back and forth between the primary wave and higher harmonics. Nonlinear interactions of the primary and spurious waves result in the modulation of the waveform.

In the literature, the classical Boussinesq equations were used to study triad interactions of periodic waves in shallow water by Mei and Ünlüata (1972), Bryant (1973), and Dingemans (1997), and nonlinear shoaling of wave spectra by Freilich and Guza (1984). Because the accuracy of higher harmonics generated by the classical Boussinesq models is limited by the dispersion characteristics of the equations, improved Boussinesq-type equations were utilized for the study by Madsen and Sørensen (1993). Physical experiments by Goda (1967), Boczar-Karakiewicz (1972), Buhr-Hansen and Svendsen (1974), and Chapalain et al. (1992) confirm the mechanism of the harmonic generation resulting from the use of first-order wave inputs. However, all of the theoretical and experimental studies mentioned above considered only pure water waves. Current effects on nonlinear interactions in shallow water have not achieved attention in the literature.

In nature, ambient currents are often encountered by wind waves. In laboratories, however, the simultaneous simulation of waves and a current is still challenging physical wave modelers. Alternatively, the numerical wave flume based on the new Boussinesq-type equations for the fully coupled wave/current interaction introduced by Chen et al. (1998) and Madsen and Schäffer (1998) offers an approach to the study of wave current interaction, including wave blocking and current effects on harmonic generation and nonlinear interactions of shallow-water waves.

This paper is organized as follows: First, we derive a set of evolution equations on the basis of the Yoon and Liu (1989) equations with a constant water depth and an ambient current. The interaction coefficients and phase mismatch of the equations with the presence of an ambient current are then compared with those of pure wave motion, which reveals the tendency of the current effects on the nonlinear interactions. Second, we briefly describe an enhanced Boussinesq model with higher dispersion accuracy for a fully coupled wave/current interaction. Emphasis is given to the treatment of the nonreflective boundary condition for the combined wave/current motion and the comparison of numerical results with labora-

[1]Post-doctoral Res. Fellow, Ctr. for Appl. Coast. Res., Univ. of Delaware, Newark, DE 19716.

[2]Prof., Dept. of Mathematical Modeling, Technical University of Denmark, DK-2800, Lyngby, Denmark.

[3]Prof. and Dir., Coast. Engrg. Ctr., Dept. of Civ. and Envir. Engrg., Old Dominion Univ., Norfolk, VA 23529-2941.

Note. Discussion open until January 1, 2000. To extend the closing date one month, a written request must be filed with the ASCE Manager of Journals. The manuscript for this paper was submitted for review and possible publication on March 5, 1998. This paper is part of the ***Journal of Waterway, Port, Coastal, and Ocean Engineering***, Vol. 125, No. 4, July/August, 1999. ©ASCE, ISSN 0733-950X/99/0004-0176–0186/$8.00 + $.50 per page. Paper No. 17944.

tory data. The next section starts with the analysis of the current effects on the beat-length and the second-order amplitude coefficient of the near-field solution for harmonic generation on the basis of Stokes-type theory followed by the direct numerical simulation of harmonic generation on a flat bottom with an imposing and a following current. We then employ the numerical model to investigate current effects on bound waves resulting from nonlinear shoaling and the release of higher harmonics due to the abrupt change in the water depth such as the wave passage over a submerged bar bathymetry. The blockage of higher harmonics by a strong opposing current is also presented. Finally, we summarize the findings.

CURRENT EFFECTS ON TRIAD-INTERACTION COEFFICIENTS

To obtain insight into the influence of an ambient current on near-resonant triad interactions, we derive the evolution equations on the basis of Boussinesq-type equations for a wave/current interaction with constant water depth using the multiscale method as followed by Mei and Ünlüata (1972) and Dingemans (1997). The set of equations introduced by Yoon and Liu (1989) is chosen as the starting point of our analysis for simplicity, although enhanced equations for a wave/current interaction with Padé [4, 4] dispersion characteristics exist [see Chen et al. (1998) and Madsen and Schäffer (1998)].

The one-dimensional version of the model equations on a horizontal bed is given by

$$\eta_t + hU_x + (\eta U)_x = 0 \tag{5}$$

$$U_t + UU_x + g\eta_x - \frac{1}{3}h^2U_{xxt} - \frac{1}{3}h^2UU_{xxx} = 0 \tag{6}$$

where U denotes the depth-averaged velocity in the x-direction; and η = free surface elevation. Notice that the final term in (6) is simplified from the original one, $-1/3h^2(UU_{xx})_x$, on the basis of the scaling analysis for the combined wave/current motion, as detailed in Chen et al. (1998). The additional terms introduced by Chen et al. (1998) have been neglected here because the still water level is considered as the free surface of the uniform, ambient current on a flat bed. In other words, η is the free surface due to the wave motion only.

We assume that the waveform modulation resulting from nonlinear interactions of wave components (harmonics) is much slower than the spatial variation of the free surface described by Stokes first-order waves. Consider two scales

$$x \text{ and } X = \varepsilon x \tag{7}$$

where X denotes the slow scale and the nonlinear parameter ε = the ratio of wave amplitude to still water depth ($a/h \ll 1$). Thus

$$U = U(x, X, t); \quad \eta = \eta(x, X, t) \tag{8a,b}$$

Eqs. (5) and (6) become

$$\eta_t + hU_x + \varepsilon hU_X + (\eta U)_x + \varepsilon(\eta U)_X = 0 \tag{9}$$

$$U_t + UU_x + \varepsilon UU_X + g\eta_x + \varepsilon g\eta_X - \frac{1}{3}h^2U_{xxt} - \varepsilon\frac{2}{3}h^2U_{Xxt} - \frac{1}{3}h^2UU_{xxx} - \varepsilon h^2UU_{Xxx} = 0(\varepsilon^2) \tag{10}$$

Eqs. (9) and (10) are in dimensional form, where ε indicates the slow scale of the wave modulation.

The free surface elevation η and the velocity U are expanded as power series in terms of the expansion parameter ε. They read

$$\eta(x, X, t) = \varepsilon\eta_1(x, X, t) + \varepsilon^2\eta_2(x, X, t) + \cdots \tag{11}$$

$$U(x, X, t) = U^c + \varepsilon U_1(x, X, t) + \varepsilon^2U_2(x, X, t) + \cdots \tag{12}$$

where U^c = ambient current velocity; and U_i and η_i (i = 1, 2 . . .) = depth-averaged velocity and free surface elevation due to the wave motion, respectively. The substitution of (11) and (12) into (9) and (10) leads to a hierarchy of equations. The first- and second-order equations may be expressed by

$$\begin{bmatrix} m_{11} & m_{12} \\ m_{21} & m_{22} \end{bmatrix} \begin{bmatrix} \eta_1 \\ U_1 \end{bmatrix} = \begin{bmatrix} 0 \\ 0 \end{bmatrix} \tag{13}$$

where

$$m_{11} = \frac{\partial}{\partial t} + U^c\frac{\partial}{\partial x}; \quad m_{12} = h\frac{\partial}{\partial x}; \quad m_{21} = g\frac{\partial}{\partial x} \tag{14a–c}$$

$$m_{22} = \frac{\partial}{\partial t} + U^c\frac{\partial}{\partial x} - \frac{1}{3}h^2\frac{\partial^3}{\partial x^2\partial t} - \frac{1}{3}h^2U^c\frac{\partial^3}{\partial x^3} \tag{15}$$

$$\begin{bmatrix} m_{11} & m_{12} \\ m_{21} & m_{22} \end{bmatrix} \begin{bmatrix} \eta_2 \\ U_2 \end{bmatrix} = \begin{bmatrix} f_1 \\ f_2 \end{bmatrix} \tag{16}$$

in which

$$f_1 = -(\eta_1U_1)_x - hU_{1X} - U^c\eta_{1X} \tag{17}$$

$$f_2 = -U_1U_{1x} - g\eta_{1X} + \frac{1}{3}h^2U_1U_{1xxx} - U^cU_{1X} + \frac{2}{3}h^2U_{1xtX} + h^2U^cU_{1xxX} \tag{18}$$

We consider the solution to (13), consisting of three harmonic components, as

$$\eta_1 = \sum_{j=1}^{3} a_j(X)e^{i\phi_j} + * \tag{19}$$

$$U_1 = \sum_{j=1}^{3}\left(\frac{\omega_j - U^ck_j}{k_jh}\right)a_j(X)e^{i\phi_j} + * \tag{20}$$

where a_j = amplitude; k_j = wave number; $*$ denotes the complex conjugate of the foregoing terms; and

$$\phi_j = k_jx - \omega_jt \tag{21}$$

in which the absolute angular frequency is given by

$$\omega_1 = \omega; \quad \omega_2 = 2\omega; \quad \omega_3 = 3\omega \tag{22a–c}$$

The requirement of the nontrivial solution of (13) yields the linear dispersion relations as

$$(\omega_j - U^ck_j)^2 = \sigma_j^2, \quad j = 1, 2, 3 \tag{23}$$

where the intrinsic angular frequency is given by

$$\sigma_j^2 = \frac{k_j^2gh}{1 + \frac{1}{3}(k_jh)^2} \tag{24}$$

Solving (16) leads to

$$(m_{11}m_{22} - m_{12}m_{21})\eta_2 = f_1m_{22} - f_2m_{12} \tag{25}$$

$$m_{11}m_{22} - m_{12}m_{21})U_2 = f_2m_{11} - f_1m_{21} \tag{26}$$

If we consider that η_2 and U_2 have solutions similar to the form of (19) and (20), the requirement of a bounded second-order solution leads to

$$f_1m_{22} - f_2m_{12} = 0 \tag{27}$$

$$f_2m_{11} - f_1m_{21} = 0 \tag{28}$$

Eqs. (27) and (28) are identical. They essentially prevent the second-order solution from containing harmonics common to the first-order solution. This is the so-called solubility con-

straint in the literature [e.g., Freilich and Guza (1984)]. Inserting (19) and (20) into (27) and applying the solubility constraint to each harmonic component lead to the evolution equations as

$$\frac{da_1}{dX} = -i\,\frac{Q_1}{S_1}\,a_1^* a_2 e^{i(\phi_2-2\phi_1)} - i\,\frac{P_1}{S_1}\,a_2^* a_3 e^{i(\phi_3-\phi_2-\phi_1)} \tag{29}$$

$$\frac{da_2}{dX} = -i\,\frac{Q_2}{S_2}\,a_1^2 e^{i(2\phi_1-\phi_2)} - i\,\frac{P_2}{S_2}\,a_1^* a_3 e^{i(\phi_3-\phi_2-\phi_1)} \tag{30}$$

$$\frac{da_3}{dX} = -i\,\frac{P_3}{S_3}\,a_1 a_2 e^{i(\phi_1+\phi_2-\phi_3)} \tag{31}$$

where

$$S_j = 2g\sigma_j\left(1 - \frac{1}{3}\frac{h}{g}\sigma_j^2\right) + 2gU^c k_j, \quad j = 1, 2, 3 \tag{32a}$$

$$Q_1 = \frac{g}{h}(k_2 - k_1)^2\left(\frac{\sigma_1}{k_1} + \frac{\sigma_2}{k_2}\right) + \frac{1}{h^2}\sigma_1\sigma_2\left(\frac{1}{k_1} - \frac{1}{k_2}\right)(\sigma_2 - \sigma_1) + \frac{1}{3}\sigma_1\sigma_2\left(\frac{k_2^2}{k_1} - \frac{k_1^2}{k_2}\right)(\sigma_2 - \sigma_1) \tag{32b}$$

$$P_1 = \frac{g}{h}(k_3 - k_2)^2\left(\frac{\sigma_2}{k_2} + \frac{\sigma_3}{k_3}\right) + \frac{1}{h^2}\sigma_2\sigma_3\left(\frac{1}{k_2} - \frac{1}{k_3}\right)(\sigma_3 - \sigma_2) + \frac{1}{3}\sigma_2\sigma_3\left(\frac{k_3^2}{k_2} - \frac{k_2^2}{k_3}\right)(\sigma_3 - \sigma_2) \tag{32c}$$

$$Q_2 = \frac{4g}{h}\sigma_1 k_1 + \frac{2}{h^2}\frac{\sigma_1^3}{k_1} + \frac{2}{3}\sigma_1^3 k_1 \tag{32d}$$

$$P_2 = \frac{g}{h}(k_3 - k_1)^2\left(\frac{\sigma_1}{k_1} + \frac{\sigma_3}{k_3}\right) + \frac{1}{h^2}\sigma_1\sigma_3\left(\frac{1}{k_1} - \frac{1}{k_3}\right)(\sigma_3 - \sigma_1) + \frac{1}{3}\sigma_1\sigma_3\left(\frac{k_3^2}{k_1} - \frac{k_1^2}{k_3}\right)(\sigma_3 - \sigma_1) \tag{32e}$$

$$P_3 = \frac{g}{h}(k_1 + k_2)^2\left(\frac{\sigma_1}{k_1} + \frac{\sigma_2}{k_2}\right) + \frac{1}{h^2}\sigma_1\sigma_2\left(\frac{1}{k_1} + \frac{1}{k_2}\right)(\sigma_1 + \sigma_2) + \frac{1}{3}\sigma_1\sigma_2\left(\frac{k_2^2}{k_1} + \frac{k_1^2}{k_2}\right)(\sigma_1 + \sigma_2) \tag{32f}$$

and a_j^* = complex conjugate of a_j. Q_1, P_1, and P_2 are subharmonic transfers, whereas Q_2 and P_3 are superharmonic transfers.

Comparison of the evolution equations for the combined wave/current motion and the pure wave motion (Dingemans 1997) indicates that both sets of equations have identical form, but the corresponding coefficients are different. An ambient current influences nonlinear interactions in two ways. First, the Doppler shift has overall effects on the wave number, resulting in the changes in wave phase mismatches and the interaction coefficients. Second, an ambient current has a direct influence on the interaction coefficients, as shown by S_j. The additional terms in Q_1, P_1, Q_2, P_2, and P_3 of the evolution equations for the combined wave/current motion result from the Boussinesq-like term for the wave/current interaction in Yoon and Liu's (1989) equations. It is apparent that the extent of the current effects depends on the strength of an ambient-current velocity and the wave period. When the current dies out, the present set of interaction coefficients becomes identical to that in Dingemans [(1998, p. 809, Eqs. (7.2a–e)], except the additional terms, that is, the third terms in Q_1, P_1, Q_2, P_2, P_3, and the scaling factors.

To estimate the influence of a current on triad interactions, we consider the simple case where the third harmonic a_3 is absent and the first harmonic $a_1(x)$ is constant. In this case, the analytical solution to (30) yields

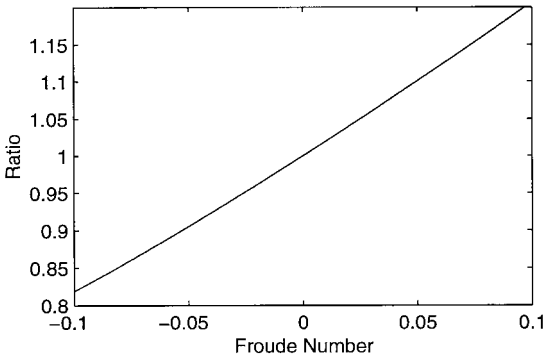

FIG. 1. Illustration of Current Effect on Second Harmonic Transfer Relative to that of Pure Wave Motion with $h/L_0 = 0.03$

$$a_2 = \frac{Q_2}{S_2\delta_2}\,a_1^2 e^{-i\delta_2 x} \tag{33}$$

It is therefore of interest to determine the transfer function $Q_2/(S_2\delta_2)$ with and without currents. In Fig. 1, this transfer function is shown relative to the corresponding value of pure waves as a function of the Froude number [$\mathsf{F} = U^c/\sqrt{(gh)}$]. The primary wave is assumed to be of $h/L_0 = 0.03$ [$L_0 = g/(2\pi)T^2$]. Consequently, the second harmonic has $h/L_0 = 0.12$, which is within the applicable range of Yoon and Liu's (1989) equations when F is equal to -0.1. We notice that a following current (positive Froude number) increases the magnitude of the second harmonic, whereas an opposing current (negative Froude number) decreases the magnitude. This indicates that an opposing current will reduce the extent of triad interactions, and that a following current will intensify triad interactions.

NUMERICAL WAVE FLUME FOR COMBINED WAVE/CURRENT MOTION

It was shown by Chen et al. (1998) that the dispersion accuracy of Yoon and Liu's (1989) equations is limited to small wave numbers and weak opposing currents. Consequently, Chen et al. (1998) and Madsen and Schäffer (1998) introduced new sets of Boussinesq-type equations with Padé [4, 4] dispersion characteristics for wave/current interaction. A numerical model on the basis of the new set of equations (given in Appendix I) was developed by Madsen et al. (1996) and Banijamali (1997), who made use of quasi-fourth-order finite-difference schemes similar to those in Wei et al. (1995). A detailed analysis of the numerical schemes in a staggered grid system and validation of the model for the case of pure wave motion can be found in Banijamali (1997). We adapt this model for the present study by the incorporation of nonreflective boundary conditions for the fully coupled wave and current motion.

It is well known that difficulties exist in physical experiments for modeling the combined wave and current motion because of the problems with input and output boundaries of waves and currents. Similar to the problem in physical modeling, the absorption of combined waves and currents is more difficult than radiating pure shortwaves or pure currents in numerical models. Various techniques appear in the literature for radiating pure shortwaves (dispersive) and pure long waves (nondispersive) or currents. Unfortunately, no method exists for the absorption of both shortwaves and currents together. The strategy we propose is to couple two known methods—the sponge layer concept suitable for shortwaves and the Sommerfeld radiation condition for long waves—to benefit from their different but complementary properties.

The method for absorbing shortwaves is based on the sponge layer technique introduced by Larsen and Dancy

(1983). Instead of attenuating the surface elevation and fluid velocity to zero at the end of the sponge layer as in pure wave models, we dampen shortwaves with respect to a reference level. A subroutine for attenuation is called at each time step after the iteration convergence criteria are met in the model. Inside the sponge regime, the dependent variables are attenuated in the following manner:

$$\eta_j = \eta_{ref} + (\eta_j - \eta_{ref})/C_s \tag{34}$$

$$u_j = u_{ref} + (u_j - u_{ref})/C_s \tag{35}$$

in which the subscript *ref* denotes the reference value; and C_s = damping coefficient function defined by

$$C_s = \alpha_s^{\gamma_s^{(i-1)}}, \quad i = 1, 2, \ldots n \tag{36}$$

where α_s and γ_s = two free parameters. Numerical experiments suggest that $\alpha_s = 2$, $\gamma_s = 0.88-0.92$, and $n = 50-100$ lead to the efficient absorption of shortwaves while allowing currents to pass through for the simulation in the present work. The damping coefficients for optimal absorption are somewhat case-sensitive. The length of the sponge layer is usually taken to be one or two times the typical wavelength. With this sponge length, long waves or currents are able to penetrate through the sponge layer and reach the boundary. By the choice of the variables' values at the boundary as the attenuation references, the currents or long waves will not be affected by the sponge layer.

The Sommerfeld radiation condition is then utilized to allow long waves or currents to leave the computational domain. The condition can be expressed by

$$\eta_t + c\eta_x = 0 \tag{37}$$

where η = surface elevation of the combined wave and current motion; and c = outgoing wave celerity. In this case, c is taken to be the long wave celerity. The combination of (37) with the mass equation on a flat bottom leads to

$$u_\alpha \approx U = \frac{c\eta}{h + \eta} \tag{38}$$

$$c = \sqrt{g(h + \eta)} \tag{39}$$

in which u_α = velocity at an arbitrary elevation. The model equations (see Appendix I) are formulated in terms of u_α and η. In the case of long waves or currents, the effects of surface curvature are negligible.

As the first-order approximation, we estimate the surface elevations at the boundary and outside the computational domain by linear extrapolation. The linear extrapolation is justified by the fact that very fine resolution is usually involved with long waves in the case of modeling the combined shortwave and current motion. Detailed implementation of the nonreflective boundary condition can be found in Chen (1997). We obtain the needed boundary values for spatial discretization of the equations at the boundary by the use of the mixed fourth- and second-order schemes for spatial derivatives. Fortunately, the linear extrapolation does not cause any instability problem. It is concluded from numerical experiments (Chen 1997; Chen et al. 1998) that the combination of the sponge layer and Sommerfeld radiation condition works efficiently for radiating coupled shortwaves and currents in the time-domain Boussinesq models.

The effectiveness is illustrated by the numerical simulation in Fig. 2, where a wave envelope is shown. A channel 20 m in length and 1.0 m in water depth is utilized for the numerical test. At the center of the channel (i.e., $x = 10$ m), a wave/current maker internally generates two steady, constant currents with a magnitude of 0.313 m/s in two opposite directions. Two radiating boundaries are applied at both ends of the channel. This results in an increase of 0.105 m in the free surface elevation when the flow reaches the steady state. The water depth from the free surface of the channel is now 1.105 m. At the western boundary, we impose a sinusoidal wave train on top of the opposing current by replacing the radiation boundary with a wavemaker boundary. The incoming wave has a period of 5 s and an initial height of 0.02 m. The Froude number of the flow is about 0.1. In the portion $0 < x < 10$ m of the channel, the wave propagates against the current. In contrast, the wave train travels on a following current in the portion of $10 < x < 20$ m of the channel. A sponge layer with

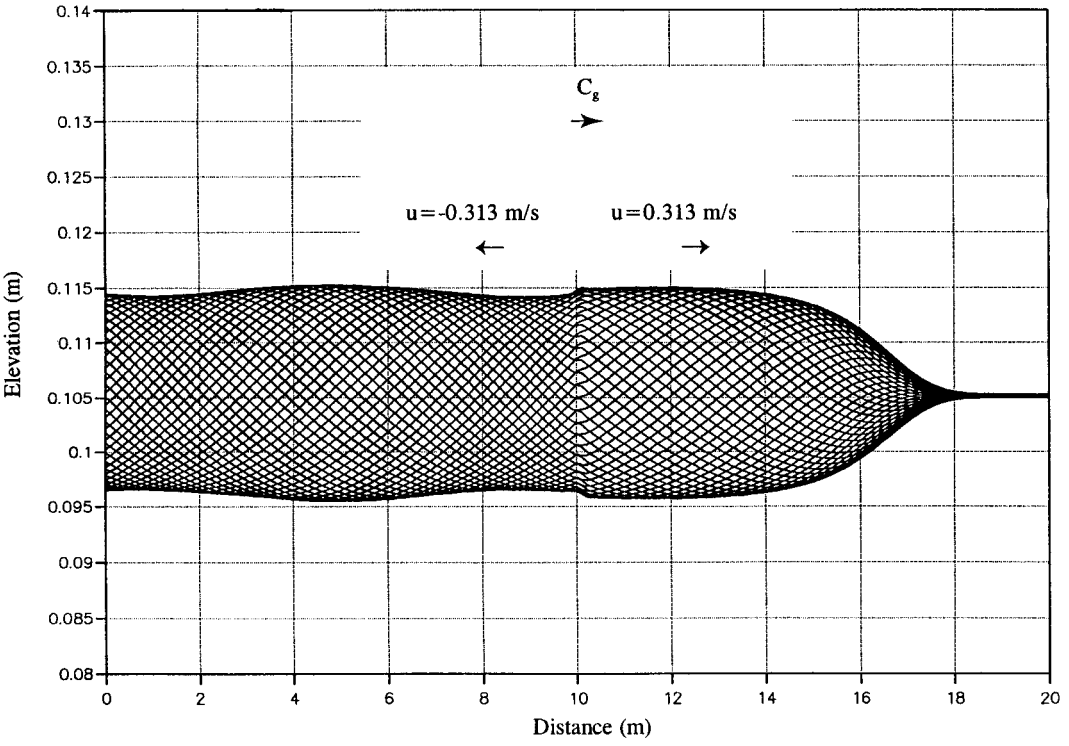

FIG. 2. Illustration of Effectiveness of Nonreflective Boundary Condition for Fully Coupled Wave and Current Motion

a length of 8 m and a radiating condition are applied at the eastern boundary. The 5-s waves are efficiently attenuated by the sponge layer while the current is allowed to leave the computational domain without reflection. However, weak reflection is observed in the portion $0 < x < 10$ m, resulting from the velocity discontinuity at the center of the channel due to the internal current generation. In this test, the grid spacing and the time step are chosen to be 0.1 m and 0.01 s, respectively.

Next, the numerical model is verified against physical experiment data in the absence of ambient currents. We consider the experiments on wave propagation over a submerged bar bathymetry. The laboratory data were measured by Luth et al. (1994). These data were simulated by Madsen et al. (1996), and excellent agreement was found. Only one test case is chosen here for illustration, as shown in Fig. 3.

A submerged bar topography as shown in Fig. 3(a) is employed in the numerical wave flume, which is 32 m long and 0.4 m deep. The water depth on the crest of the bar is 0.1 m. The western and eastern slopes of the bar are 1/20 and 1/10, respectively. As a monochromatic wave train propagates over the underwater bar, on the upward slope, wave shoaling generates bound harmonics that propagate with the primary wave. It is well known that the higher harmonics start to be released as free waves after the passage of the bar crest due to the increase in water depth. On the downward slope, the difference between the primary wave and free higher harmonics becomes clearly visible because they travel at different wave celerities. A model/data comparison for a wave train with 2.0 s in period and 0.01 m in initial amplitude over the submerged bar bathymetry is presented in Figs. 3(b and c). The dotted lines represent the computed amplitudes of the first four harmonics that agree well with the physical experimental results obtained by Luth et al. (1994). In the numerical model we used a sponge layer on the eastern boundary. This leads to an efficient absorption of wave energy as no reflected waves were observed in the numerical results.

Because there is a lack of laboratory data available for model verification in the case of combined wave/current motion over the varying topography, the linear solution based on the wave action principle was used to test the model and excellent agreement was found, as demonstrated by Chen et al. (1998). The validated time-domain Boussinesq model suitable for the combined wave/current motion shall be used for the

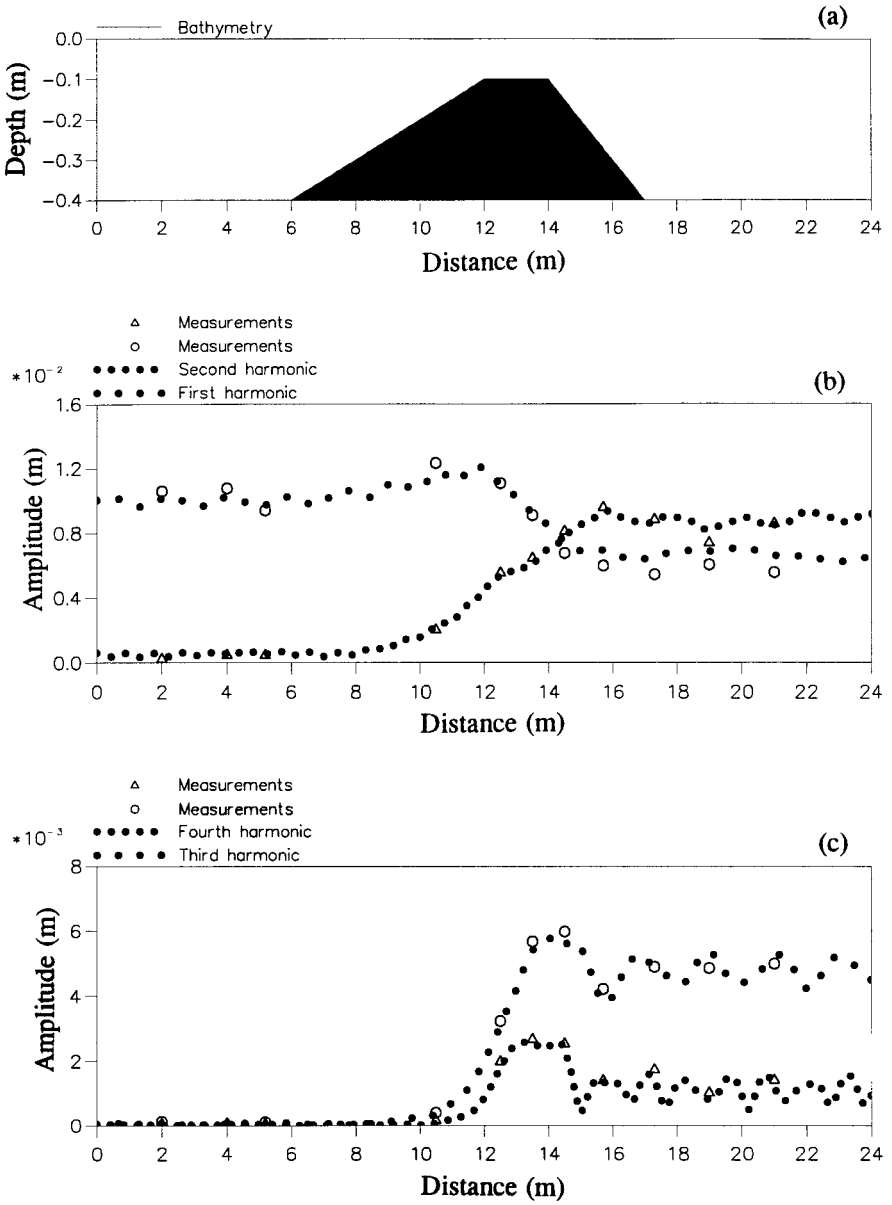

FIG. 3. Comparison of Computed Harmonic Amplitudes (Dotted Lines) and Measurements (Circles and Triangles): (a) Topography; (b) First and Second Harmonics; (c) Third and Fourth Harmonics

numerical investigation of current effects on nonlinear interactions of shallow-water waves in the following sections.

HARMONIC GENERATION ON FLAT BOTTOM WITH CURRENTS

As in the case of pure wave motion, harmonic generation on a flat bottom with ambient currents due to the use of first-order input boundary conditions can be readily illustrated by the superposition of the bound waves and free, spurious waves. Baddour and Song (1990) obtained the Stokes-type third-order solution for waves on an uniform current. The surface elevation is expressed as

$$\eta = a_1 \cos(kx - \omega t) + a_2 \cos 2(kx - \omega t) + a_3 \cos 3(kx - \omega t) \tag{40}$$

where the second-order amplitude a_2, the third-order amplitude a_3, and the first-order dispersion relation are, respectively, given by

$$a_2 = G_2 \frac{a_1^2}{h}; \quad a_3 = G_3 \frac{a_1^3}{h^2} \tag{41a,b}$$

in which

$$G_2 = \frac{kh}{4} \frac{(2 + \cosh 2kh)\cosh kh}{\sinh^3 kh} \tag{42a}$$

$$G_3 = \frac{3(kh)^2}{64} \frac{(1 + 8\cosh^6 kh)}{\sinh^6 kh} \tag{42b}$$

$$(\omega - U^c k)^2 = \sigma^2 \tag{43}$$

in which

$$\sigma^2 = gk \tanh kh \tag{44}$$

The use of first-order boundary conditions leads to the release of parasitic higher harmonics [see, e.g., Goda (1967) and Madsen and Sørensen (1993)], which are of equal amplitude and opposite phase compared with the bound waves. If we neglect the interactions between the primary wave and free, spurious waves and only consider the superposition of the bound and free harmonics, at third-order the resulting free surface elevation may be expressed by

$$\eta(x, t) = a_1 \cos(k_1 x - \omega_1 t) + a_2(x)\sin\left[(2k_1 + k_2)\frac{x}{2} - 2\omega_1 t\right] a_3(x)\sin\left[(3k_1 + k_3)\frac{x}{2} - 3\omega_1 t\right] \tag{45}$$

in which

$$a_2(x) = 2G_2 \frac{a_1^2}{h} \sin\left(\frac{\delta_2 x}{2}\right) \tag{46}$$

$$a_3(x) = 2G_3 \frac{a_1^3}{h^2} \sin\left(\frac{(\delta_2 + \delta_3)x}{2}\right) \tag{47}$$

where the mismatches are defined as

$$\delta_2 = k_2 - 2k_1 \tag{48}$$

$$\delta_3 = k_3 - k_2 - k_1 \tag{49}$$

The wave numbers are determined by the dispersion relation [(43) and (44)]. In the case of a small wave number, (45) with (46) and (47) can be found as analytical solutions to the evolution equations [(29)–(31)].

Eqs. (45)–(49) indicate that an ambient current influences the waveform modulation mainly through the Doppler shift effect on the phase mismatch. Figs. 4 and 5 illustrate the current effects on the beat-length ($L_{b2} = 2\pi/\delta_2$) and the second-order amplitude coefficient G_2. Given $h/L_0 = 0.03$, 0.04, and 0.05, and $-0.15 \leq F \leq 0.15$, we compute the ratios of L_{b2} and G_2 taken relative to the corresponding values without currents as depicted in Figs. 4 and 5 as a function of the Froude number. It is noted that an opposing current reduces the beat-length and the energy exchange between the primary wave and higher harmonics, and vice versa for a following current. For example, as $F = -0.15$ and $h/L_0 = 0.04$, the near-field solution with the opposing current predicts a reduction of about 68% in the beat-length and 24% in second-order amplitude in comparison with the case without currents. Although these values may be overestimates of the current effects due to the limitation of the Stokes-type expansion in shallow water, they give the tendency and order to magnitude of the current effects.

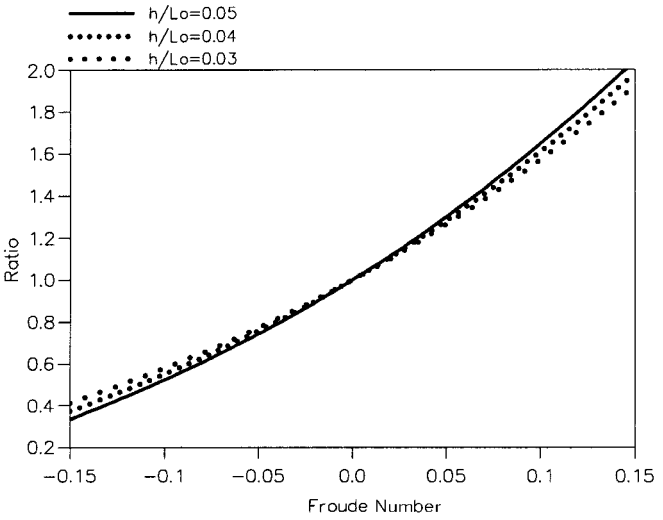

FIG. 4. Illustration of Current Effect on Ratio of Beat-Length L_{b2} Relative to that of Pure Wave Motion

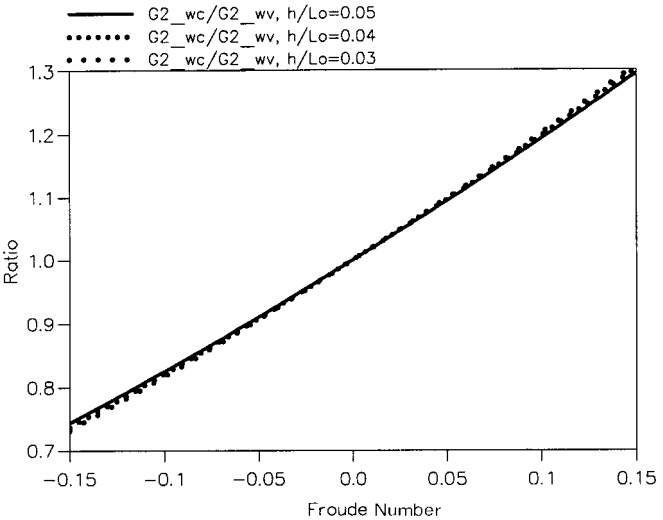

FIG. 5. Illustration of Current Effect on Ratio of Second-Order Amplitude Coefficient G_2 Relative to that of Pure Wave Motion

To accurately describe the phenomena of harmonic generation and nonlinear interactions, evolution equations as derived in the preceding section are required. In the present study, however, instead of solving the evolution equations, we use the time-domain Boussinesq model as described in the previous section to investigate the influence of an ambient current on harmonic generation.

First of all, we simulate the harmonic generation on a flat bed in the absence of an ambient current. The channel is 38 m long and 0.4 m deep. The grid spacing and time step are chosen as 0.04 m and 0.01 s, respectively. At the western

boundary of the channel, a first-order boundary condition with 2.5 s in wave period and 0.084 m in wave height is imposed, which generates spurious free higher-order waves resulting in the modulation of the wave train along the channel. A sponge layer is employed at the eastern boundary where the wave energy is efficiently absorbed. This test case without ambient currents shall be used as a benchmark to illustrate the offset resulting from current effects. As the next step, steady, uniform flows with the Froude numbers $F = \pm 0.15$ are generated, and then first-order boundary conditions with the corresponding current velocity are imposed at the western boundary. The water depth of the channel, wave period, and wave height are kept identical to those for the case of the pure wave motion. A sponge layer that allows currents to pass through is employed at the eastern boundary. Fourier analyses of the model results reveal the amplitude of each harmonic varying along the channel. Fig. 6(a–c) show the amplitudes of the first three harmonics corresponding to the cases of the following current, quiescent water, and opposing current, respectively. Currents with the typical strength of $|F| = 0.15$ have significant effects on the harmonic generation. The following current lengthens the beat-length by ~86% and increases the second-order amplitude by ~20% in comparison with those of the pure wave motion. On the other hand, the opposing current results in a reduction of ~57% in beat-length and ~14% in the second-order amplitude. In other words, a following current intensifies the extent of energy exchange between harmonics, and vice versa for an opposing current, as illustrated in Fig. 6.

Although currents change the incoming wave height, the three test cases described above employed the same first-order amplitude to highlight the current effects on the harmonic generation. The next two test cases will include the influence of the change in the first-order amplitude due to an ambient current. We repeat the tests with a following and an opposing current, but replace the incident first-order wave heights by 0.071 and 0.104 m, respectively, which are determined by the wave action balance equation. The resultant Ursell numbers are found to be 34.1 and 24.8, respectively. In comparison with the Ursell number of 29.5 for the case of pure wave motion, the following current with $F = 0.15$ increases the Ursell number by ~16%, even though the first-order wave height is reduced. In contrast, the opposing current with $F = 0.15$ decreases the Ursell number by ~16% while the first-order wave height is increased. Figs. 7(a and c) show the first three harmonics of the modeled waves on the following and opposing currents, respectively. The harmonics for the pure wave motion are again presented as a reference [Fig. 7(b)]. The model results indicate that although the amplitude of the second harmonic is reduced by the following current because of the reduction of the first-order amplitude, the ratio of the energy in the second harmonic to the energy in the primary wave is increased, and vice versa for the case of opposing current. This tendency is in agreement with the theoretical predictions as illustrated in Figs. 1, 4, and 5.

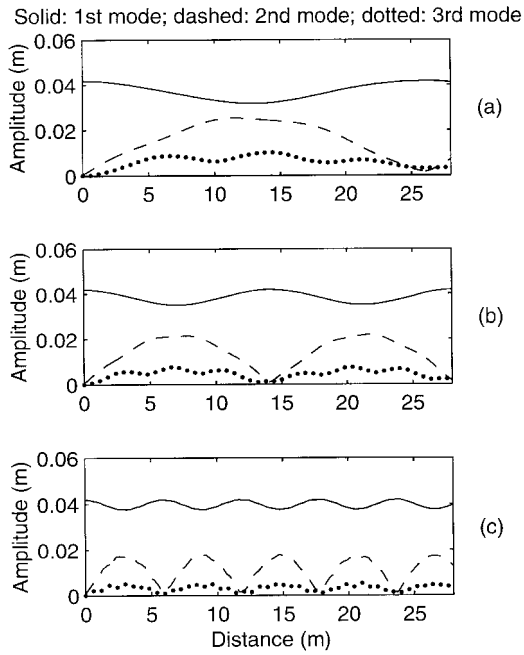

FIG. 6. Amplitudes of First Three Harmonics Generated with Same Incident Wave Height in Cases of: (a) Following Current; (b) Quiescent Water; (c) Opposing Current

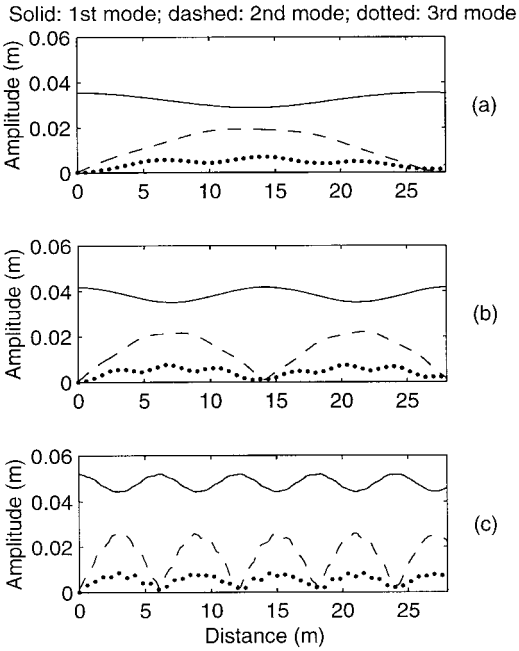

FIG. 7. Amplitudes of First Three Harmonics Generated in Cases of: (a) Following Current; (b) Quiescent Water; (c) Opposing Current. Incident Wave Heights of Primary Waves Are Determined Based on Wave Action Conservation Principle

CURRENT EFFECTS ON NONLINEAR SHOALING

We consider the simplest case of monochromatic propagation over a submerged bar with ambient currents. The current influences on the higher harmonics generated by nonlinear shoaling are numerically investigated. The same submerged bar topography as shown in Fig. 3(a) and the same model setup are employed in the numerical experiments.

First of all, steady flows over the submerged bar topography are generated by using the model. Initially, we impose a constant velocity of -0.025 m/s at the eastern boundary and a radiating condition at the western boundary. This leads to a steady current flowing from the east to the west of the channel. The resulting water level on the flat bed of the channel is 0.005 m, whereas on the crest of the bar it becomes 0.0045 m. Unlike the simulation of current blocking, no bottom friction is used in the channel in this case. The velocity on top of the bar reaches the maximum strength of -0.102 m/s and the resultant Froude number is ~ -0.1. Fig. 8 shows the computed stationary spatial variation of the velocity and the surface elevation. As demonstrated in Chen et al. (1998), the modeled steady flow agrees well with the result of nonlinear shallow water equations neglecting the vertical acceleration of the flow, because the effect of the surface curvature of the flow is minor.

Next, we impose a sinusoidal wave train on top of the steady current field. The incident wave period of 2.0 s is identical to that in the absence of a current. The corresponding

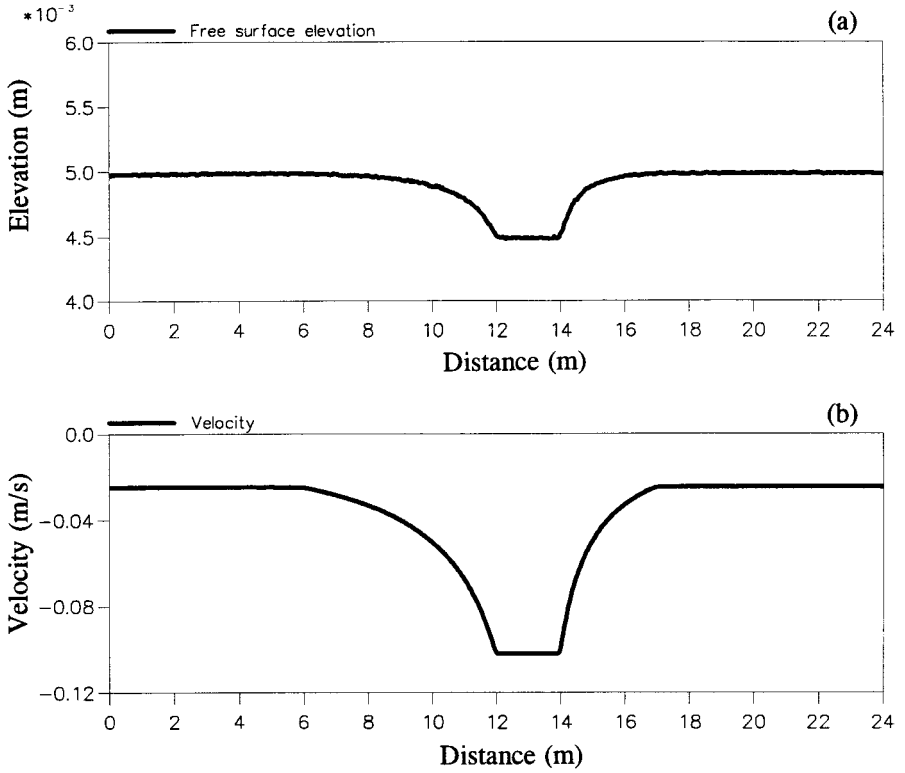

FIG. 8. Computed Spatial Variation of Surface Elevation and Particle Velocity of Steady, Open Channel Flow: (a) Free Surface Elevation; (b) Velocity at *z*-Elevation (*z* = 0.541 h)

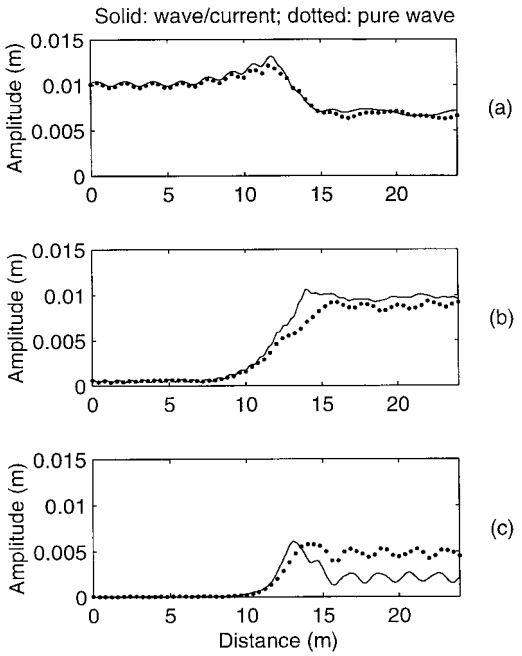

FIG. 9. Comparison of Harmonics of Monochromatic Wave Train Traveling over Submerged Bar with Opposing Current and without Current: (a) First Harmonics; (b) Second Harmonics; (c) Third Harmonics

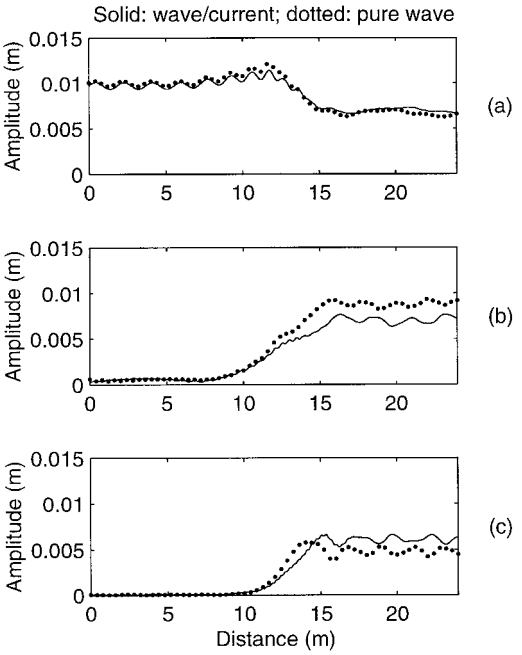

FIG. 10. Comparison of Harmonics of Monochromatic Wave Train Traveling over Submerged Bar with Following Current and without Current: (a) First Harmonics; (b) Second Harmonics; (c) Third Harmonics

wave height applied on the western boundary with a current velocity of −0.025 m/s is equal to 0.206 m. We choose the grid size and the time step to be 0.04 m and 0.01 s, respectively. The results of a Fourier analysis of the computed surface elevation are presented in Fig. 9, where the amplitudes of the first three harmonics are compared with those in the absence of a current. On the western slope of the submerged bar, the opposing current increases the amplitudes of the primary and bound higher harmonics compared with the case of pure wave motion. On the crest of the bar, higher harmonics start to be released as free waves, which become more sensitive to an ambient current and the beat-length governs the energy transfer between the primary and higher harmonics. As shown in the preceding section, an opposing current shortens the beat-length. The higher harmonics therefore exchange energy with the primary wave more quickly due to the presence of the opposing current. After the passage over the bar, higher harmonics become free waves that are exposed to more current effects than the bound harmonics.

We repeat the preceding simulation, but change the direction

of the current. Fig. 10 shows the resultant amplitudes of the first three harmonics for wave propagating on the following current over the submerged bar. Once again, the corresponding amplitudes for the case of pure wave motion are also presented for comparison. Phenomena as contrasted to those for an opposing current are observed from Fig. 10. A following current decreases the amplitudes of the primary and bound higher harmonics of shoaling waves. When waves pass the bar crest, a longer distance is involved with the exchange of energy between the primary and higher harmonics on a following current in comparison with the case of pure wave motion. We notice that the following current slightly intensifies the extent of interactions among the free second-harmonic and other wave components, and vice versa for the opposing current.

Chen et al. (1998) studied shoaling waves blocked by strong, opposing currents using a similar submerged bar topography with milder slopes (i.e., 1/50 for the western slope and 1/20 for the eastern slope) as shown in Fig. 11(a). They concluded that higher harmonics are not blocked as long as they are bound to the primary wave, which has a stronger group velocity than the current speed. We repeat the same numerical simulation here to take a close look at the current effect on shoaling. First, a spatially varying, opposing current with a Froude number $F = -0.4$ on the crest of the submerged bar is generated. We then impose a monochromatic wave train with a period of 2.4 s on the current field, which is strong enough to block a 1.2-s wave train near the crest of the bar, as demonstrated by Chen et al. (1998). The incoming wave height is 0.02 m on the western boundary.

Fig. 11 shows the variation of the computed first and second harmonics along the channel. As a reference, the corresponding amplitudes of the pure wave propagation are also presented. The opposing current significantly increases the magnitude of the primary wave on the upward slope ($7 < x < 37$ m) and gradually blocks the second harmonic on the downward slope ($41 < x < 53$ m), where the attenuation of the primary wave is attributed to the bottom friction used in that region for simulation of the flow. Although the amplitude of the second harmonic is also larger than that of the pure wave motion, the ratio ($R = a_2^2/a_1^2$) of the energy in the second harmonic to the energy of the primary wave is actually reduced by the opposing current in comparison with the case of pure wave motion. At the location of $x = 35$ m, for example, the opposing current decreases the energy ratio R by ~27%. This indicates that an opposing current may reduce the degree of asymmetry and skewness of shoaling waves when com-

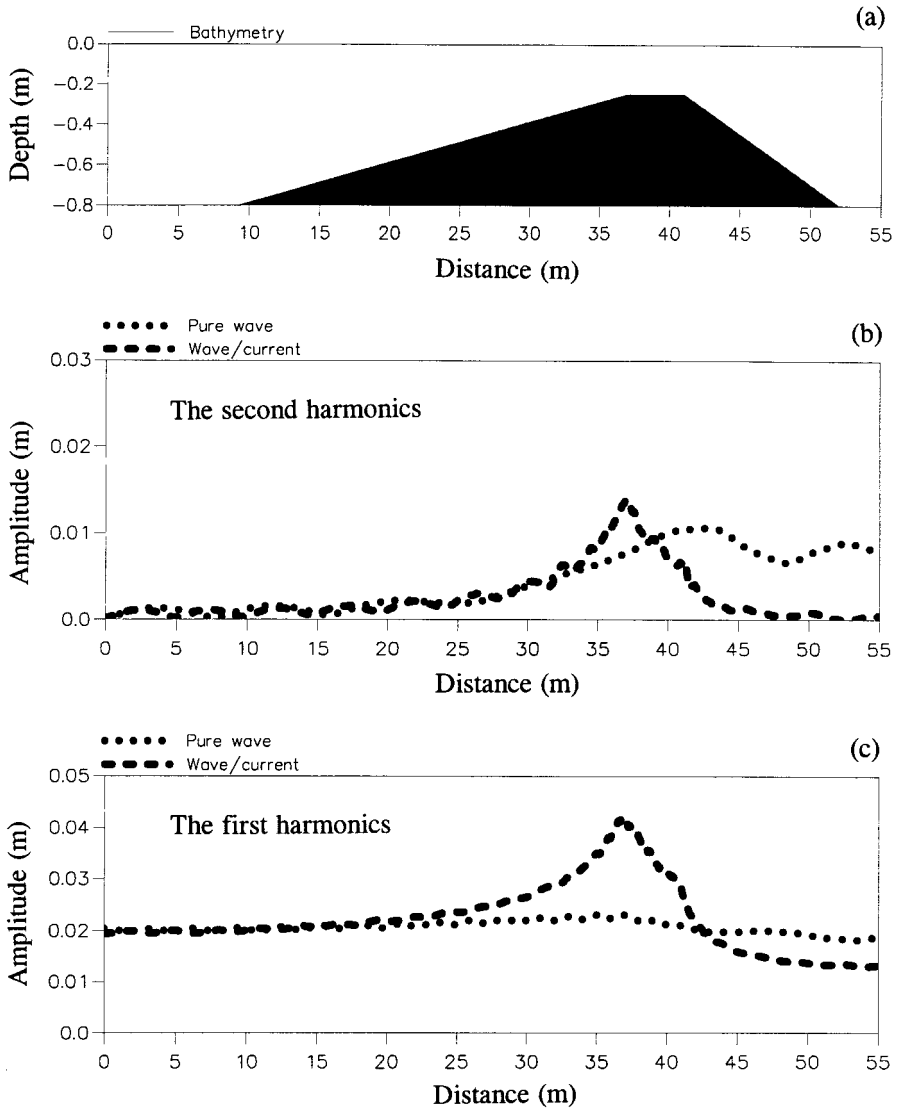

FIG. 11. Simulation of Monochromatic Waves Propagating over Submerged Bar Topography with Spatially Varying Opposing Current (Dashed Lines) and without Current (Dotted Lines): (a) Topography; (b) Amplitudes of Second Harmonics; (c) Amplitudes of First Harmonics

pared with the wave of the same height in the absence of a current.

SUMMARY AND CONCLUSIONS

In this paper, current effects on nonlinear interactions of shallow-water waves were investigated. First, evolution equations for near-resonant triad interactions on an ambient current with a constant water depth were derived and analyzed. Insights into the current effects on shallow-water wave interactions were gained through the comparison of the interaction coefficients and the transfer function with those in the case of pure wave motion. Second, the near-field solution on the basis of a Stokes-type third-order theory was obtained and utilized to examine the current effects of the beat-length and second-order amplitude. Third, a nonreflective boundary condition for the fully coupled wave/current motion were incorporated into a Boussinesq model. This permits us to use the model as a research tool to numerically investigate the current effects.

In the numerical experiments, the enhanced Boussinesq model with highly accurate dispersion properties for the fully coupled wave/current motion was employed to simulate the harmonic generation and propagation of nonlinear water waves over a submerged bar topography with ambient currents. It can be concluded from the theoretical analyses and numerical experiments that an opposing current will reduce the Ursell number, the beat-length, and the ratio of the energy in the higher harmonics to the energy in the primary wave, and vice versa for a following current. In other words, an opposing current will diminish the extent of triad interactions while a following current will intensify energy exchange between wave components. This is in complete, direct contrast to the current effects on deepwater waves.

From the shoaling tests it was also found that an ambient current had less effect on bound harmonics than on free harmonics. The free higher-order waves may exchange energy with the primary wave within a shorter distance in the case of an opposing current because the beat-length is reduced. If the opposing current is stronger than the free-wave intrinsic group velocity, the released harmonics will be blocked.

APPENDIX I. MODEL EQUATIONS

The numerical model in this paper is based on Madsen and Schäffer's (1998) equations as follows:

$$\eta_t + \nabla\cdot\mathbf{Q} = 0 \tag{50}$$

where

$$\mathbf{Q} = (h+\eta)\left[\mathbf{u}_\alpha + \left(\frac{z_\alpha^2}{2} - \frac{1}{6}(h^2 - h\eta + \eta^2)\right)\nabla(\nabla\cdot\mathbf{u}_\alpha) + \left(z_\alpha + \frac{1}{2}(h-\eta)\right)\nabla(\nabla\cdot(h\mathbf{u}_\alpha))\right] + (\beta_2 - \beta_1)h^2\nabla(\nabla\cdot((h+\eta)\mathbf{u}_\alpha)) - \beta_2\nabla(h^2\nabla\cdot((h+\eta)\mathbf{u}_\alpha)) + (\beta_2 - \beta_1)h^2\nabla\eta_t - \beta_2\nabla(h^2\eta_t) \tag{51}$$

$$\mathbf{u}_{\alpha t} + (\mathbf{u}_\alpha\cdot\nabla)\mathbf{u}_\alpha + g\nabla\eta + \mathbf{\Lambda}_0 + \mathbf{\Lambda}_1 + \mathbf{\Lambda}_2 + \mathbf{\Lambda}_3 = 0 \tag{52}$$

where

$$\mathbf{\Lambda}_0 = \left(\frac{z_\alpha^2}{2} + (\alpha_2 - \alpha_2)h^2\right)\nabla(\nabla\cdot\mathbf{u}_{\alpha t}) + (z_\alpha - \alpha_2 h)\nabla(\nabla\cdot(h\mathbf{u}_{\alpha t})) + (\alpha_2 - \alpha_1)h^2\nabla(\nabla^2\eta) - \alpha_2 h\nabla(\nabla\cdot(h\nabla\eta)) \tag{53}$$

$$\mathbf{\Lambda}_1 = \nabla\left[z_\alpha(\mathbf{u}_\alpha\cdot\nabla)(\nabla\cdot(h\mathbf{u}_\alpha)) + \frac{1}{2}z_\alpha^2(\mathbf{u}_\alpha\cdot\nabla)(\nabla\cdot\mathbf{u}_\alpha) - \eta\nabla\cdot(h\mathbf{u}_{\alpha t}) + \frac{1}{2}(\nabla\cdot(h\mathbf{u}_\alpha))^2\right] + \frac{1}{2}(\alpha_2 - \alpha_1)h^2\nabla(\nabla^2(\mathbf{u}_\alpha^2)) - \frac{1}{2}\alpha_2 h\nabla(\nabla\cdot(h\nabla(\mathbf{u}_\alpha^2))) \tag{54}$$

$$\mathbf{\Lambda}_2 = \nabla\left[\eta(\nabla\cdot\mathbf{u}_\alpha)(\nabla\cdot(h\mathbf{u}_\alpha)) - \eta\mathbf{u}_\alpha\cdot\nabla(\nabla\cdot(h\mathbf{u}_\alpha)) - \frac{1}{2}\eta^2\nabla\mathbf{u}_{\alpha t}\right] \tag{55}$$

$$\mathbf{\Lambda}_3 = \nabla\left[\frac{1}{2}\eta^2(\nabla\cdot\mathbf{u}_\alpha)^2 - \frac{1}{2}\eta^2\mathbf{u}_\alpha\cdot\nabla(\nabla\cdot\mathbf{u}_\alpha)\right] \tag{56}$$

in which h = still water depth; η = free surface elevation relative to the still water level; $\mathbf{u}_\alpha$ = velocity vector at the reference elevation z_α ($=-0.54122h$); the subscript t denotes time differentiation; and ∇ = horizontal gradient operator. In addition $(\beta_1, \beta_2) = (0.03917, 0.14453)$ and $(\alpha_1, \alpha_2) = (0.01052, 0.02153)$.

ACKNOWLEDGMENTS

This work was financed by the Danish National Research Foundation when the first writer was a Ph.D. student at the International Research Centre for Computational Hydrodynamics, Denmark and Old Dominion University. The manuscript was prepared by the first writer under Research Grant N00014-97-1-0283, from the Office of Naval Research. Their support is greatly appreciated. Coding assistance from Drs. Ole Sørensen and Babak Banijamali is acknowledged.

APPENDIX II. REFERENCES

Armstrong, J. A., Bloembergen, N., Ducuing, J., and Pershan, P. S. (1962). ''Interaction between light waves in a nonlinear dielectric.'' *Physical Rev., B*, 127, 1918–1939.

Baddour, R. E., and Song, S. W. (1990). ''Interaction of higher-order water waves with uniform currents.'' *Oc. Engrg.*, 17(6), 551–568.

Banijamali, B. (1997). ''A study of enhanced Boussinesq equations and their numerical modeling,'' PhD thesis, Aalborg University and International Research Center for Computational Hydrodynamics (ICCH), Danish Hydraulic Institute, Denmark.

Boczar-Karakiewicz, B. (1972). ''Transformation of wave profile in shallow water—A Fourier analysis.'' *Arch. Hydrptechnik*, 19, 197–210.

Bretherton, F. P. (1964). ''Resonant interactions between waves: The case of discrete oscillation.'' *J. Fluid Mech.*, 20, 457–480.

Bryant, P. J. (1973). ''Periodic waves in shallow water.'' *J. Fluid Mech.*, 59, 625–644.

Buhr-Hansen, J., and Svendsen, I. A. (1974). ''Laboratory generation of waves of constant form.'' *Proc., 14th Int. Conf. Coast. Engrg.*, ASCE, 320–338.

Chapalain, G., Cointe, R., and Temperville, A. (1992). ''Observed and modelled resonantly interacting progressive water waves.'' *Coast. Engrg.*, 16, 267–301.

Chen, Q., (1997). ''The study of wave-blocking and current effects on nonlinear interactions of shallow-water waves using advanced Boussinesq models,'' PhD thesis, Old Dominion University, Virginia, and International Research Centre for Computational Hydrodynamics (ICCH), Danish Hydraulic Institute, Denmark.

Chen, Q., Madsen, P. A., Schäffer, H. A., and Basco, D. R. (1998). ''Wave-current interaction based on an enhanced Boussinesq approach.'' *Coast. Engrg.*, 33, 11–39.

Dingemans, M. W. (1997). *Water wave propagation over uneven bottoms. Part 2—Non-linear wave propagation.* World Scientific, River Edge, N.J., 806–814.

Freilich, M. H., and Guza, R. T. (1984). ''Nonlinear effects on shoaling surface gravity waves.'' *Philosophical Trans. Royal Soc.*, London, A331, 1–41.

Goda, Y. (1967). *Traveling secondary wave crests in wave channels.* Technical Report, Vol. 13, Port and Harbor Research Institute, Japan, 32–38.

Hasselmann, K. (1962). ''On the non-linear energy transfer in a gravity-wave spectrum—General theory.'' *J. Fluid Mech.*, 12(1), 481–500.

Larsen, J., and Dancy, H. (1983). ''Open boundaries in short-wave simulations—A new approach.'' *Coast. Engrg.*, 7(3), 285–297.

Luth, H. R., Klopman, G., and Kitou, N. (1994). ''Project 13G: Kinematics of waves breaking partially on an offshore bar: LDV measurements for wave with and without a net offshore current.'' *Delft Hydraulics, Rep. H 1573.*

Madsen, P. A., Banijamali, B., Schäffer, H. A., and Sørensen, O. R. (1996). ''Higher order Boussinesq type equations with improved dispersion and nonlinearity.'' *Proc., 25th Int. Conf. Coast. Engrg.*, ASCE, 95–108.

Madsen, P. A., and Schäffer, H. A. (1998). ''Higher order Boussinesq-type equations: Derivation and analysis.'' *Philosophical Trans. Royal Soc.*, London, 356, 3123–3184.

Madsen, P. A., and Sørensen, O. R. (1993). ''Bound waves and triad interactions in shallow water.'' *Oc. Engrg.*, 20, 359–388.
Mei, C.-C., and Ünlüata, U. (1972). ''Harmonic generation in shallow water waves.'' *Waves on beaches*, R. E. Meyer, ed., Academic, New York, 181–202.
Phillips, O. M. (1960). ''On the dynamics of unsteady gravity waves of finite amplitude. Part 1.'' *J. Fluid Mech.*, 9, 193–217.
Wei, G., Kirby, J. T., Grilli, S. T., and Subramanya, R. (1995). ''A fully nonlinear Boussinesq model for surface waves. Part 1. Highly nonlinear unsteady waves.'' *J. Fluid Mech.*, 294, 71–92.
Yoon, S. B., and Liu, P. L.-F. (1989). ''Interaction of currents and weakly nonlinear water waves in shallow water.'' *J. Fluid Mech.*, 205, 397–419.